Full-tracking resolution in DIRAC with 2001 data

B. Adeva, A. Romero, O. Vázquez Doce

IGFAE, University of Santiago de Compostela, Spain

Abstract

The purpose of this note is to make a complete evaluation of reconstruction efficiency and resolution of the Full-Tracking method in DIRAC. This is the only method that uses the upstream arm of the spectrometer as such. The 10 upstream detectors account for a sizable amount of radiation length and the background conditions are extremely high in all of them. Monte Carlo simulation is used to evaluate in detail the critical distributions for the lifetime measurement, namely Q_X, Q_Y, Q_T and Q_L. Conditions of 2001 spectrometer data were chosen for this analysis.

DIRAC note 2005-15 *29 July 2005*

1 Introduction

The general characteristics of the full-tracking reconstruction were described in reference [1], where its global performance with real data was evaluated. Basically, it relies on the utilisation of the upstream arm of DIRAC spectrometer [2], by means of an independent pattern recognition of particle tracks, which are matched with drift chamber tracks with given charge sign and (zeroth-order) momentum. By introducing additional hits from 4 MSGC planes closest to the interation point, it could not be otherwise (for details of mathematical treatment see references [3] and [4]) that this method provides the best resolution in lambda mass and the best resolution in transverse momentum [5], [6], as compared to other drastically incomplete approaches [7].

Apart from the above-mentioned obvious merits, the real advantage of the upstream arm relies on its capability for maximal reduction of detector backgrounds and decays. This point is essential for determination of pionium lifetime with a high intensity proton beam, because when the atom signal is mapped into the (Q_T, Q_L) plane, background will be reflected into uncertainty in Q_T, and therefore into systematic error. Dropping the Q_T projection from the analysis would result, on the other hand, in reduced (statistical) precision with respect to the 2D fit.

Of course, an analysis based upon Q_L measurement only would be a perfectly consistent alternative, but then the DIRAC upstream arm becomes itself a serious limitation to Q_L resolution, unless tracking detectors are fully exploited.

2 Overview of reconstruction

A complete description of the tracking method principles can be found in [1]. We shall review here only those aspects that are new (with respect to ARIANE 304-26 version) or specially relevant for the present study. MSGC clusters are defined as a continuous string of microstrip (200 μm pitch) ADC signals above threshold. We call X/X' the MSGC planes with microstrips vertical and tilted by 5^o, respectively. Likewise Y/Y' for horizontal planes.

Upstream tracks are built when they have at least two hits in each projection, among the sets (X, X', SFD-X) and (Y, Y', SFD-Y), and they are matched with backward-extrapolated drift chamber tracks. Matching requires space and time coincidence between upstream and downstream tracks. Good timing with TOF counters is achieved by means of SFD TDC's.

Pattern recognition of tracks is achieved by searching hits in MSGC and SFD detectors that are compatible with having a common origin at the beam intersection with the target foil. Momentum-dependent space windows are open for this purpose, based upon diagonal elements of detector multiple scattering matrix [1]. In order to minimise the effect of MSGC background, strict (2σ) cuts are used to define the search spot. The calibrated mean central position of the beam at the target plane is used in this procedure (insignificant with Monte Carlo). Beam position is also used as a fit constraint for tracks with only 4 hits.

We say there is double ionisation in one track when at least one of the two intersected slabs of IH shows calibrated pulse [8] above threshold (140-170 counts), in a given projection (X or Y). Null pulses are excluded from the test.

For well separated pairs, where one of the tracks has only two hits in one projection and the other shows double ionisation, a signal in time from IH detector is further required in the former to validate the pair.

When both tracks share the same SFD hit, additional MSGC signals close to the track are searched for, and incorporated to either one of the two tracks. Wide MSGC clusters (strip multiplicity larger than 3) that are found in this procedure, are subsequently broken into two, before they get associated to the tracks. Double ionisation is required for this close-pair configuration, before it is accepted.

The above analysis for close-angle pairs still allows that unbroken MSGC clusters are shared by both tracks. In this case, clusters are split into two, under the assumption that they were produced by two particles. Splitting takes place then by means of a simple algorithm that takes the RMS of the strip-pulse distribution as most likely distance. In the case of one-strip clusters, it is necessary to add two small pulses at adjacent microstrips, in order to compensate partially for the effect of pedestal substraction.

Track pairs are finally re-fitted with a common vertex position. Calibrated mean central position of the beam is used as a constraint for tracks with only 4 hits. In the final re-fit, only MSGC information is used, in order minimise the effect of multiple scattering and SFD cross-talk.

3 Overview of Monte Carlo simulation

For both Coulomb and pionium pairs, the standard generator is used [9],[10]. Buffer files (which contain GEANT-DIRAC [11] output) were created after

generator cuts $Q_T < 8$ MeV/c and $|Q_L| < 24$ MeV/c. A simplified pre-selection pass is done, which performs the essential functions of the standard pre-selection used with real data [12], particularly the veto on large (> 6 MeV/c) Q_X or Q_Y estimated values, in the presence of SFD background.

Average radiation length of upstream detectors , which correlates with resolution performance, has been the subject of variations at the level of 10-15% with respect to standard GEANT-DIRAC values. For the sake of concreteness, the choice made in this work corresponds to the values optimised in [5] with real data. Lower values would of course mean better resolution, in all transverse momentum quantities which will be evaluated. A full discussion of this important parameter will be done elsewhere.

Upstream detector digitisations for SFD and IH are used from standard GEANT-DIRAC as provided by ARIANE 304-26 version, with options that are indicated in each case. For MSGC, some improvements were made with respect to 304-26, specially concerning background simulation. A description of the latter, as well as results showing the simulation quality for 2001 data, can be found in reference [13].

It is also in note [13] that optimum values of SFD efficiency parameters (PSC threshold, amplitude of double-pulse suppression) were precisely determined from real data, covering the full 2001 period with Ni target. SFD and IH background, as well as SFD cross-talk, have been recently incorporated to ARIANE [14]. The corresponding flux parameter (see ARIANE FFREAD datacards) has been set to 2.85, which fits reasonably well the average SFD hit multiplicities.

Concerning MSGC efficiency, the simulation parameters (in the range 0.86-0.92) were also cross-checked with real data. which show slightly better performance. The limit of full efficiency will also be discussed, for this and the other detectors.

4 Resolution study

In order to illustrate the general performance of the full tracking procedure, we made a detailed comparison between the input center-of-mass momentum components and the reconstructed output. Input is defined as the Q_i values for GEANT $\pi^+\pi^-$ pairs that emerge from the target foil [1] . These are considered as *true* values for the reconstruction procedure, and we denote them by Q_i^{gen}

[1] technically it is achieved by a GEANT cut at 1.15 cm away from the target foil position.

(generator pairs). As for the index i is concerned , we will discuss here the quantities Q_X, Q_Y , $|Q_X|$, $|Q_Y|$, $Q_T = \sqrt{Q_X^2 + Q_Y^2}$ and $|Q_L|$, as most representative. Only the last four are actually measurable by the experiment, because the charge sign becomes random at small opening angles, due to multiple scattering. Nevertheless we also include the first two, for the sake of illustration of tracking properties. In any case, let us mention that the alignment procedures include the charge conjugation symmetry as a constraint, and that the precise determination of pionium lifetime does not require any measurement of the charge sign.

It is required that the generated event passes the trigger and that the drift chambers produce one positive and one negative track, with standard χ^2 cuts. The ensemble of these pairs (P_0) is considered as the reference normalisation, for overall efficiency studies. Generic distributions of Q_i^{gen} in P_0 will be denoted by G_0 in the following.

A subset $P_1 \subset P_0$ is defined by reconstructed pairs. For every matched pair (between downstream and upstream arms) there will be a reconstructed (measured) value Q_i^{rec} and a generator (true) value Q_i^{gen}. In the next section we analyse the difference $|Q_i^{gen}| - |Q_i^{rec}|$ (which we call *resolution*), as well as the correlation between Q_i^{gen} and Q_i^{rec}, for atom pairs and for Coulomb pairs separately. We will be calling, generically, G_1 and R_1 the distributions of Q_i^{gen} and Q_i^{rec}, respectively, for pairs that belong to P_1.

The following results are presented after a cut $Q_T^{gen} > 6$ MeV/c , where the generator value Q_T^{gen} is defined past the target foil.

4.1 Atom pairs

In figure 1 the reconstructed Q_X distribution (R_1) is shown for atom pairs, and it is compared with generator (true) values G_1. The effects of statistical bias and efficiency, on the one hand, and distortion caused by the measurement, on the other hand, can be reasonably decoupled by showing the ratios G_1/G_0 and R_1/G_1, separately, which is done in figure 2 (top).

Figures 3 and 4 show exactly the same histograms as figures 1 and 2, but applied to Q_Y. According to these results, the following general features of $Q_{X,Y}$ reconstruction for atom pairs can be extracted:

a) there is a small overall inefficiency (less than 3%). It is attributed to double-pulse broadning in IH, inefficiency of SFD and MSGC detectors and to multiple scattering tails. The central region of Q_X shows a small additional depletion of 2-3%, which depends on the actual double ionisation cut used.

b) the measurement of $Q_{X,Y}$ reproduces the true spectrum (G_1) rather closely. There is however a small widening due to the entangled effect of detector backgrounds and detector inefficiency (SFD, MSGC,IH).

Correlation between Q_X^{gen} versus Q_X^{rec} is shown in figure 7 (top), for atom pairs. We see that besides the correct same-sign correlation, there is an orthogonal one due to charge confusion originated from multiple scattering in the overall spectrometer. This charge confusion is irrelevant for the lifetime measurement, which is based upon Q_T analysis. In addition, we see small horizontal and vertical lines. The former is due to atom pairs which have lost a SFD hit due to detector inefficiency. The vertical one originates mostly from background hits in SFD (apart from a very small component due to large-angle Coulomb scatters) that cause artificial opening of the atom pair. In both cases, what is seen in the plot corresponds to the remainder of what the MSGC detector could not resolve, due to its own inefficiency. A limited number of events has been run to produce this plot, in order to appreciate more clearly the proportion of vertical and horizontal lines.

Figures 5 and 6 (top) are structured in the same way as figures 1 and 2, but now applied to the transverse momentum Q_T, for atom pairs. The general features previously discussed for $Q_{X,Y}$ certainly apply for Q_T too. The resolution function R_1/G_1 for atom pairs (figure 6, top) now shows a depletion at small Q_T values, with a corresponding enhancement at the distribution tail. This effect is essentially due to MSGC background hits. Event-by-event resolution for atom pairs, defined by $|Q_i^{gen}| - |Q_i^{rec}|$, is analysed in figure 8 (top) for $|Q_X|$, $|Q_Y|$, and Q_T. It can be described by a gaussian fit with some tails, which are different on the positive and negative sides. These tails are evaluated as the fraction of events measured with $|\Delta Q_i| > 2$ MeV/c, in each case. Results, together with the σ values from the gaussian fit, are given in table 1

The resolution tails observed in figure 8 are asymmetric in all cases, due to the distinct effect of detector (SFD and MSGC) backgrounds (left side), which open up the pair, and inefficiency (right side), with the opposite trend. The effect of inefficiency is more severe for Coulomb pairs than it is for atom pairs, because of the larger transverse momentum span of the former.

Special attention has been devoted to the tail of reconstructed Q_T distribution for atom pairs, due to the fact that lifetime analysis will require a cut $Q_T < 4$ MeV/c (maximum allowed by unbiased pre-selection procedure). The fractional integral for $Q_T > 4$ MeV/c is given in table 3 for reconstructed atoms, together with the fraction obtained under the same cut for generator values, which also contribute to this region due to multiple scattering in the target foil. The difference between the previous two quantities (indicated in the last column of table 3) evaluates the fraction of lost pairs after $Q_T > 4$ MeV/c cut. Results are also indicated for an interesting 5 MeV/c cut.

Finally in figure 9 we also show $|Q_L|$ spectrum and in figure 10 the corresponding ratios and resolution plots for atom pairs, following the same line as for the previous discussion of other quantities.

Table 1
Gaussian resolution σ and fraction of events where $|Q_i^{gen}| - |Q_i^{rec}|$ is larger than 2 MeV/c, for atom pairs. Tails signs are distinguished.

	σ (MeV/c)	Tail (+) (%)	Tail (-) (%)
$\|Q_X\|$	0.11	0.12	1.68
$\|Q_Y\|$	0.12	0.14	1.73
Q_T	0.13	0.15	2.86
Q_L	0.52	2.63	2.56

Table 2
Gaussian resolution σ and fraction of events where $|Q_i^{gen}| - |Q_i^{rec}|$ is larger than 2 MeV/c, for Coulomb pairs. Tails signs are distinguished.

	σ (MeV/c)	Tail (+) (%)	Tail (-) (%)
$\|Q_X\|$	0.11	1.43	0.92
$\|Q_Y\|$	0.12	1.82	0.94
Q_T	0.12	1.68	1.26
Q_L	0.52	2.75	2.64

Table 3
Fraction of atoms pairs reconstructed with two different Q_T cuts, the corresponding fraction for the original generator values, and the difference between the two.

	tail (%)	generator (%)	loss (%)
$Q_T^{rec} > 4$ MeV/c	2.89	1.08	1.81
$Q_T^{rec} > 5$ MeV/c	1.54	0.31	1.23

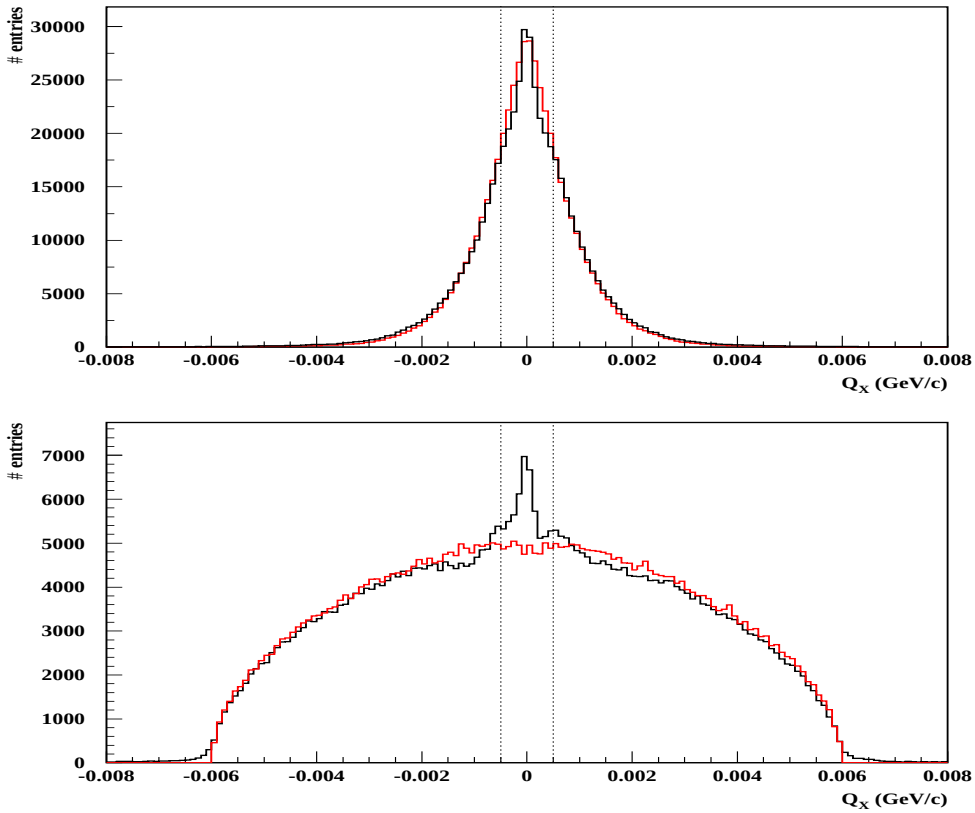

Fig. 1. *Comparison between generated Q_X spectrum G_1 (red), and reconstructed spectrum R_1 (black) for atom pairs (top), and for Coulomb pairs (bottom). See the text for more detail.*

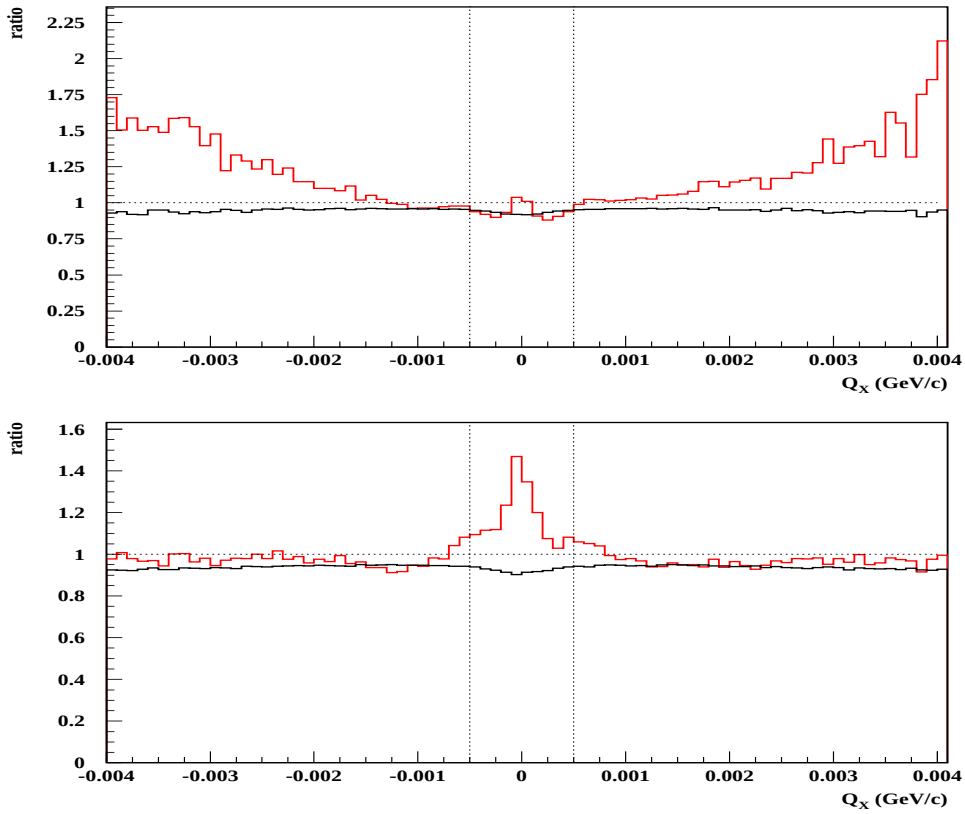

Fig. 2. *Ratios G_1/G_0 (black) and R_1/G_1 (red) for the lines shown in figure 1 for Q_X of atom pairs (top). Corresponding ratios are also given for Coulomb pairs (bottom). See text for more details.*

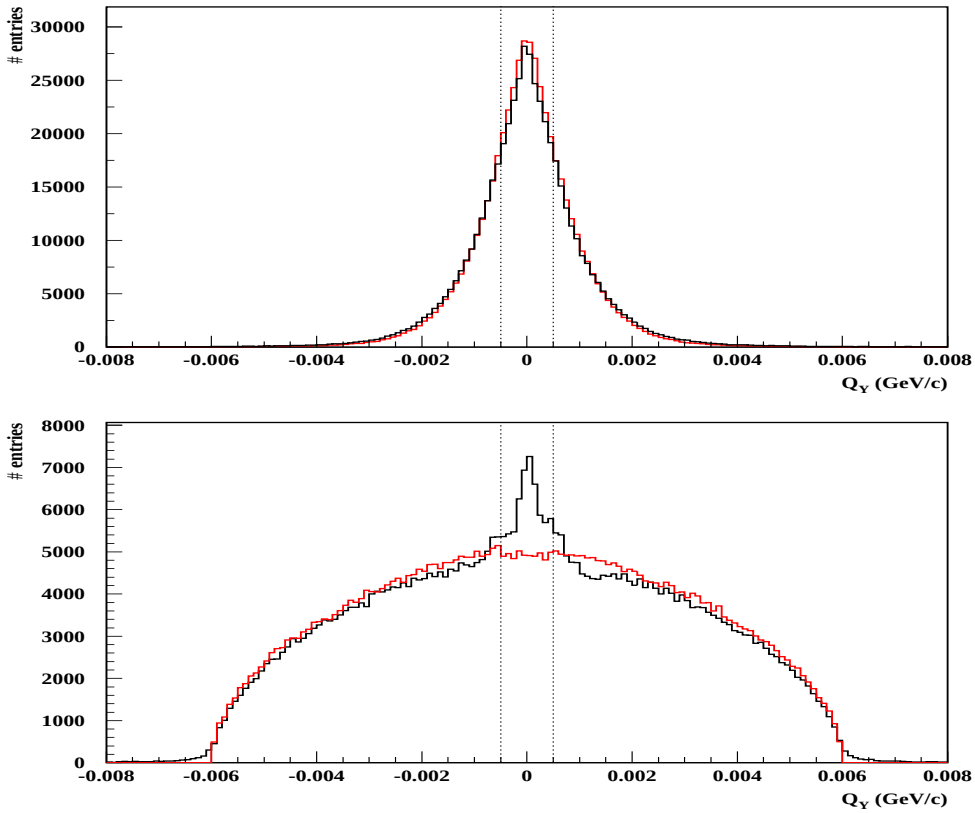

Fig. 3. *Comparison between generated values G_1 (red), and reconstructed (R_1) values (black) of Q_Y for atoms pairs (top), and for Coulomb pairs (bottom). See the text for more detail.*

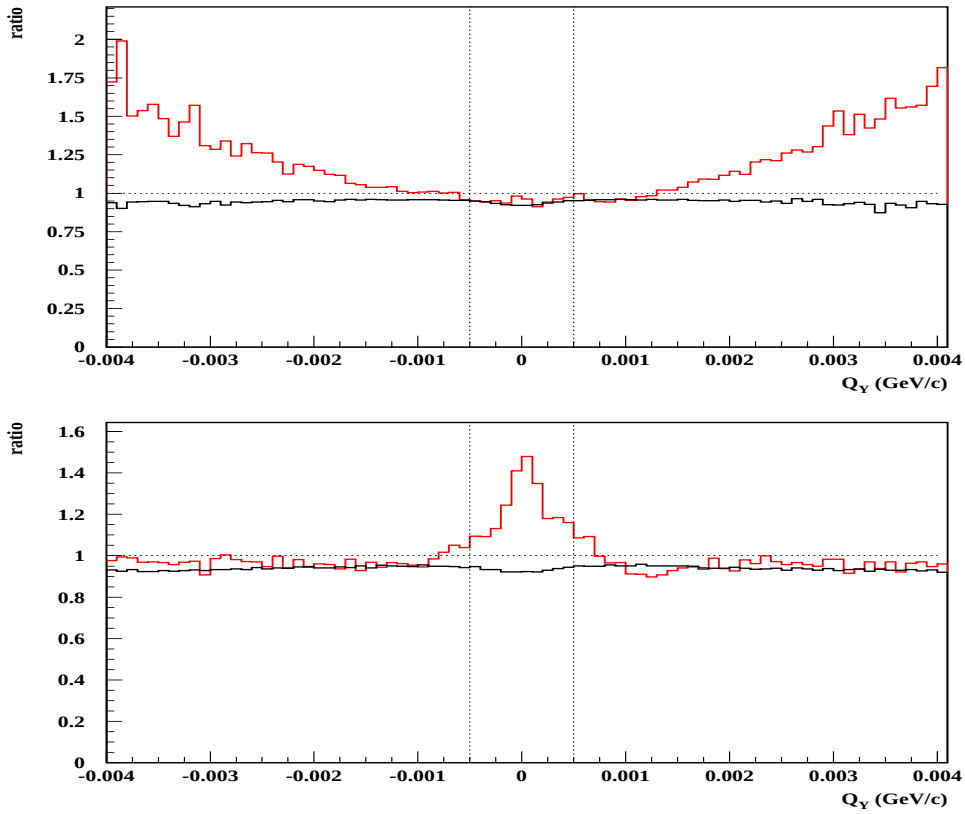

Fig. 4. *Ratios G_1/G_0 (black) and R_1/G_1 (red) for the lines shown in figure 3 for Q_Y of atom pairs (top). Corresponding ratios are also given for Coulomb pairs (bottom). See text for more details.*

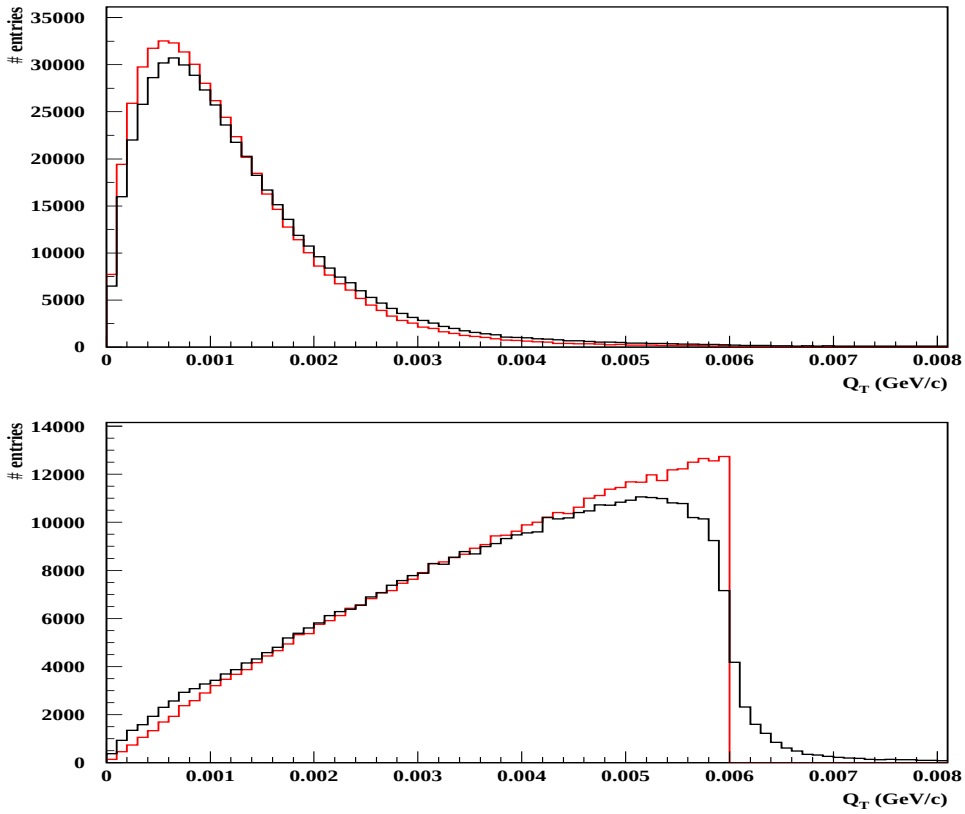

Fig. 5. *Comparison between generated Q_T spectrum G_1 (red), and reconstructed spectrum R_1 (black) for atom pairs (top), and for Coulonb pairs (bottom). See the text for more detail.*

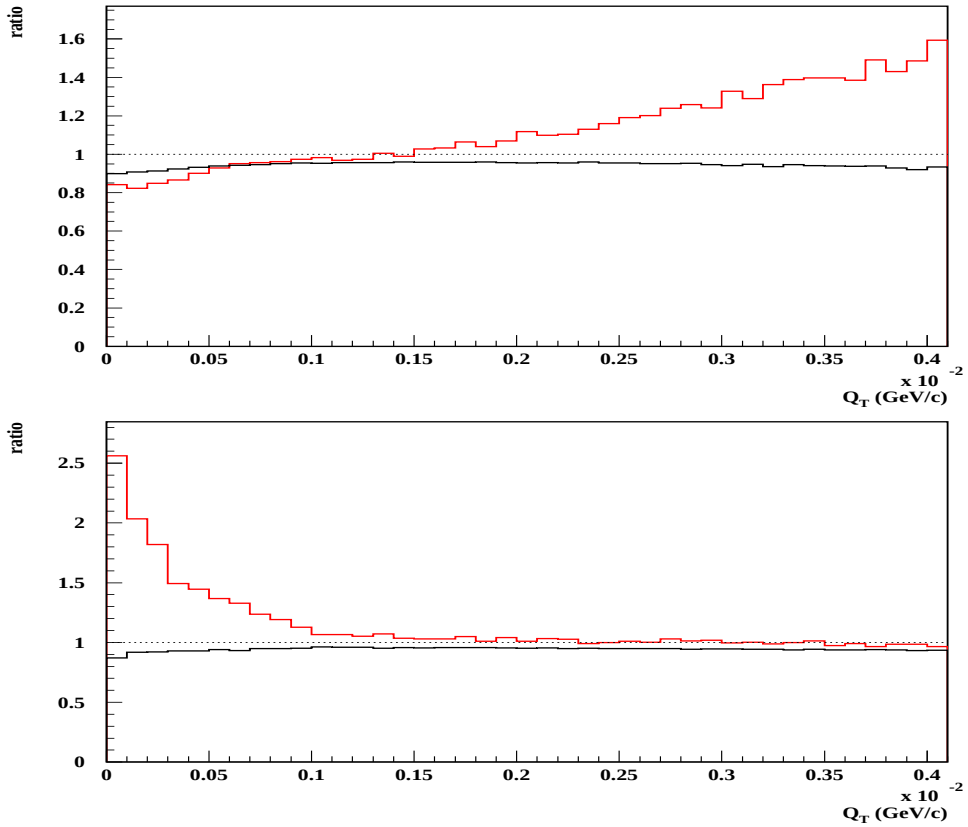

Fig. 6. *Ratios G_1/G_0 (black) and R_1/G_1 (red) for the lines shown in figure 5 for Q_T of atom pairs (top). Corresponding ratios are also given for Coulomb pairs (bottom).*

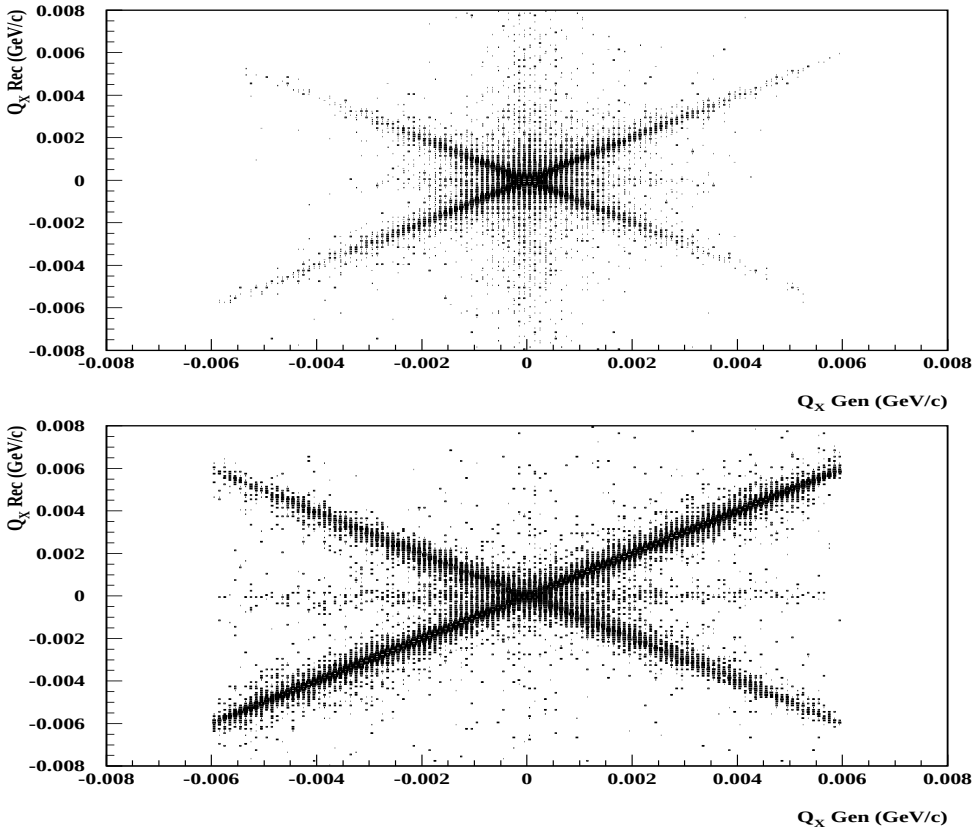

Fig. 7. *Correlation between generated and reconstructed Q_X for atoms pairs (top) and Coulomb pairs (bottom).*

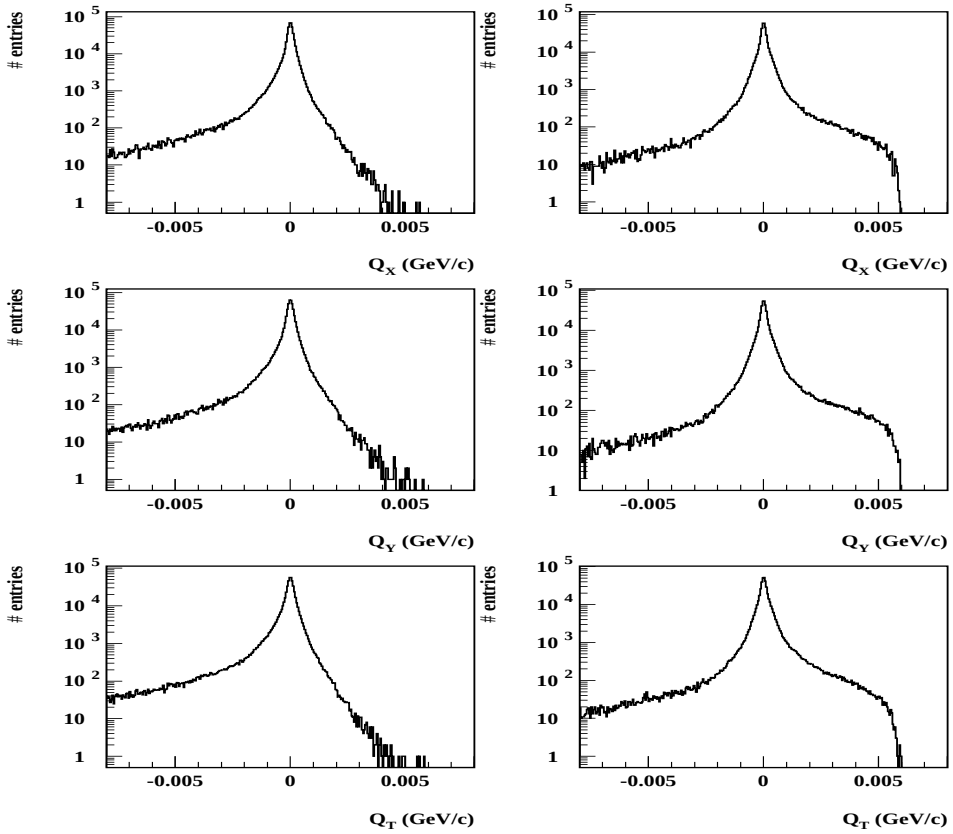

Fig. 8. *Resolution defined as* $|Q_i^{gen}| - |Q_i^{rec}|$ *for* $|Q_X|$ *(top) ,* $|Q_Y|$ *(center) and* Q_T *(bottom). Atoms pairs are shown at the left, and Coulomb pairs at the right hand side.*

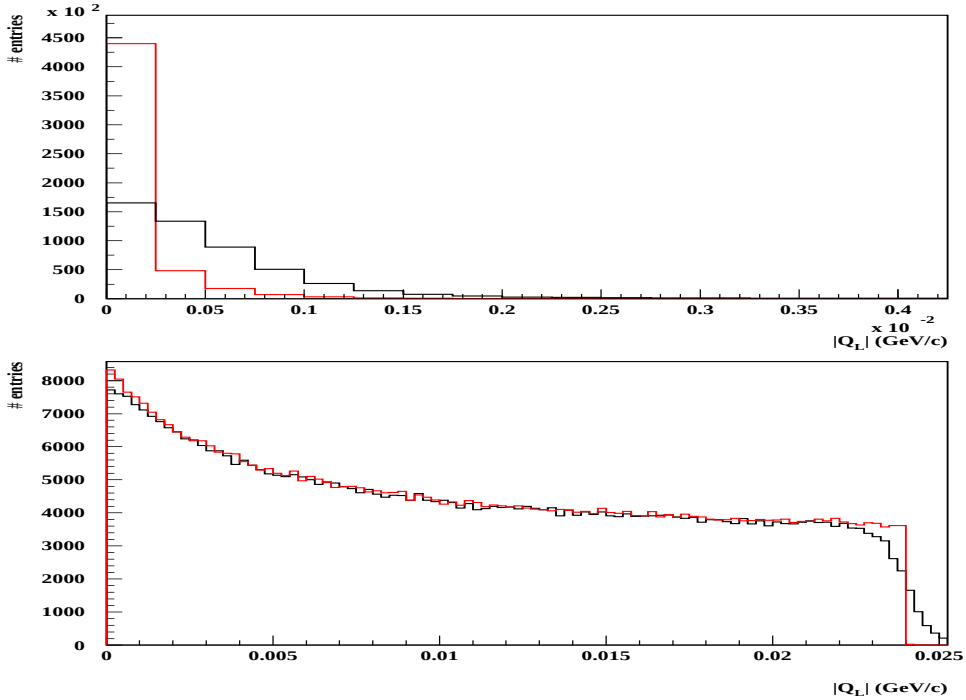

Fig. 9. *Comparison between generated $|Q_L|$ spectrum G_1 (red), and reconstructed spectrum R_1 (black) for atom pairs (top), and for Coulomb pairs (bottom).*

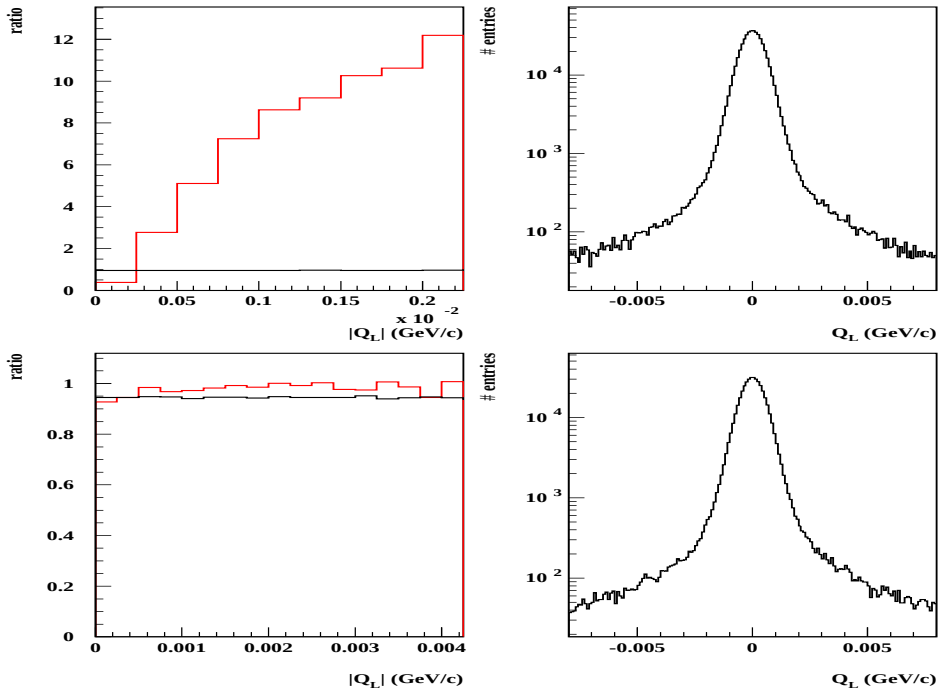

Fig. 10. *Ratios G_1/G_0 (black) and R_1/G_1 (red) for the lines shown in figure 9 for $|Q_L|$ of atom pairs (top left). and for Coulomb pairs (bottom left). Resolution plots for Q_L are also shown at the right hand side.*

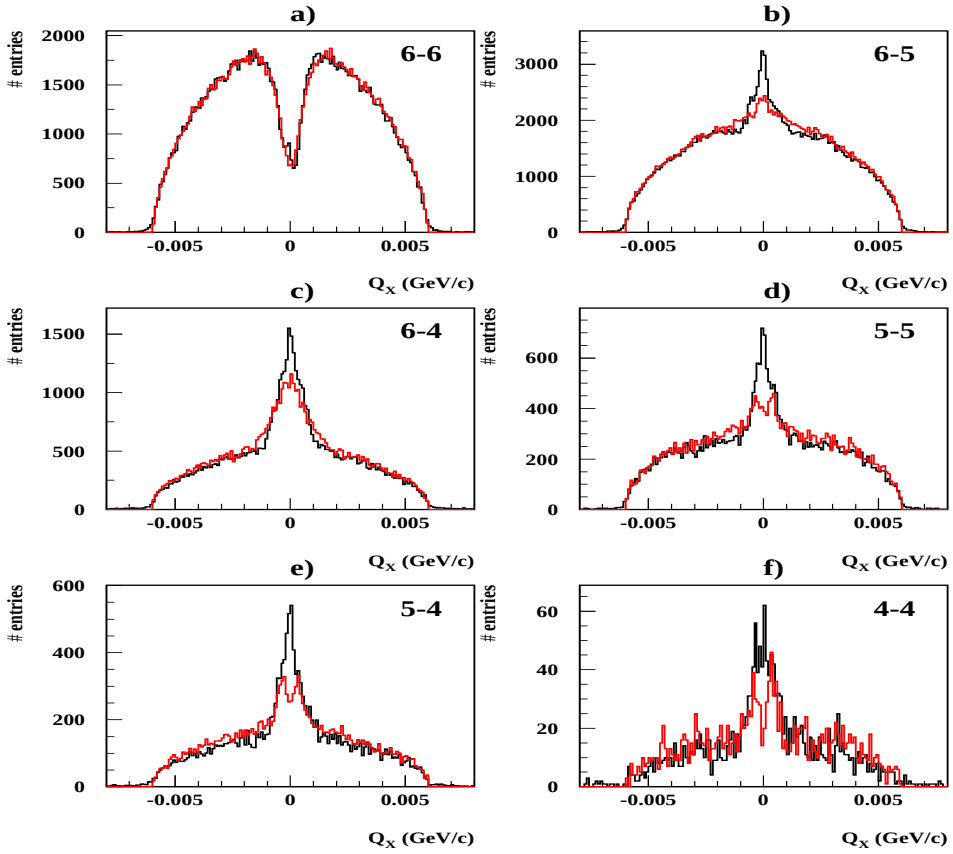

Fig. 11. *Q_X spectrum of the reconstructed Coulomb pairs shown in figure 1 (bottom) separated into 6 categories according to the number of hits in each track, namely : 6-6 , 6-5 , 6-4 , 5-5 , 5-4 , 4-4.*

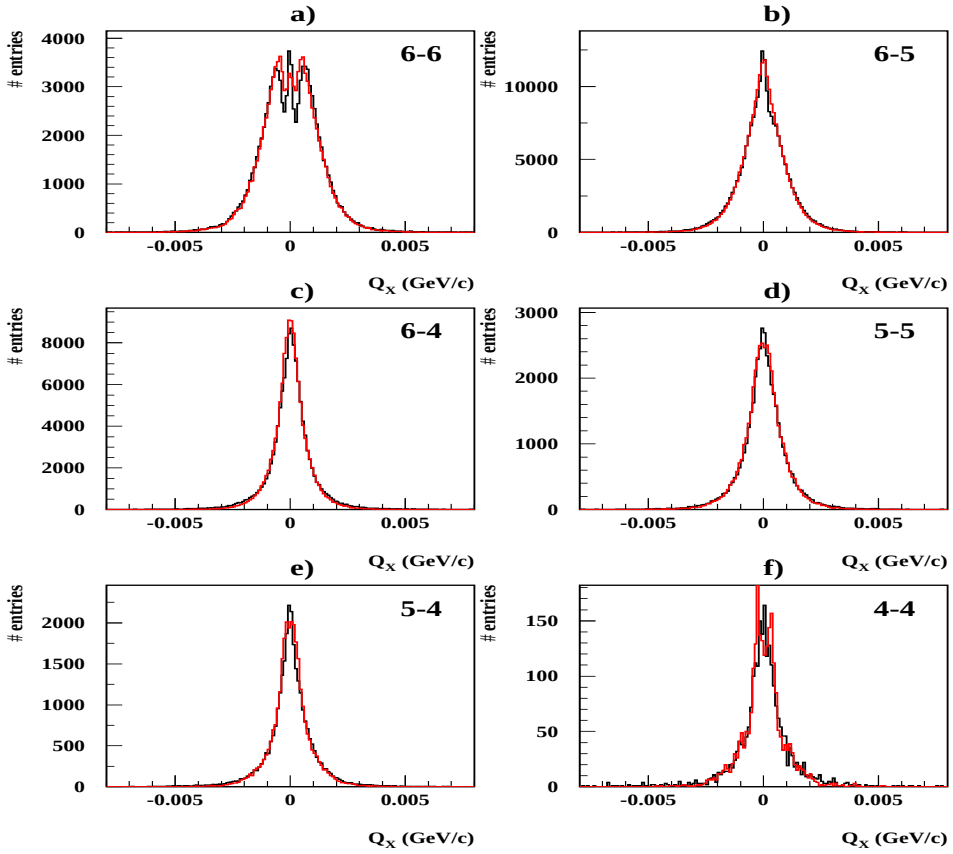

Fig. 12. *Q_X spectrum of reconstructed atom pairs shown in figure 1 (top) , separated into 6 categories according to the number of hits in each track, namely : 6-6, 6-5 , 6-4 , 5-5 , 5-4 , and 4-4.*

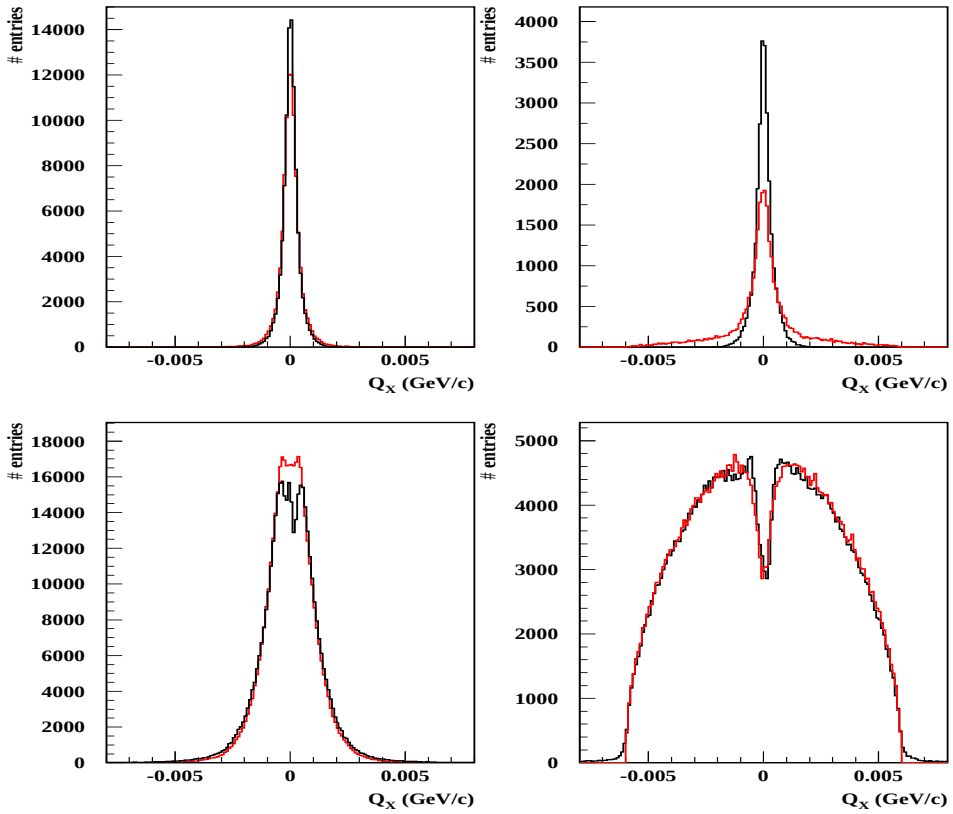

Fig. 13. *Reconstructed Q_X (black) along with generated G_1 spectrum (red) for events with a single SFD hit shared by both tracks (top), and for the remainder (bottom). Left hand side for atom pairs, right for Coulomb pairs.*

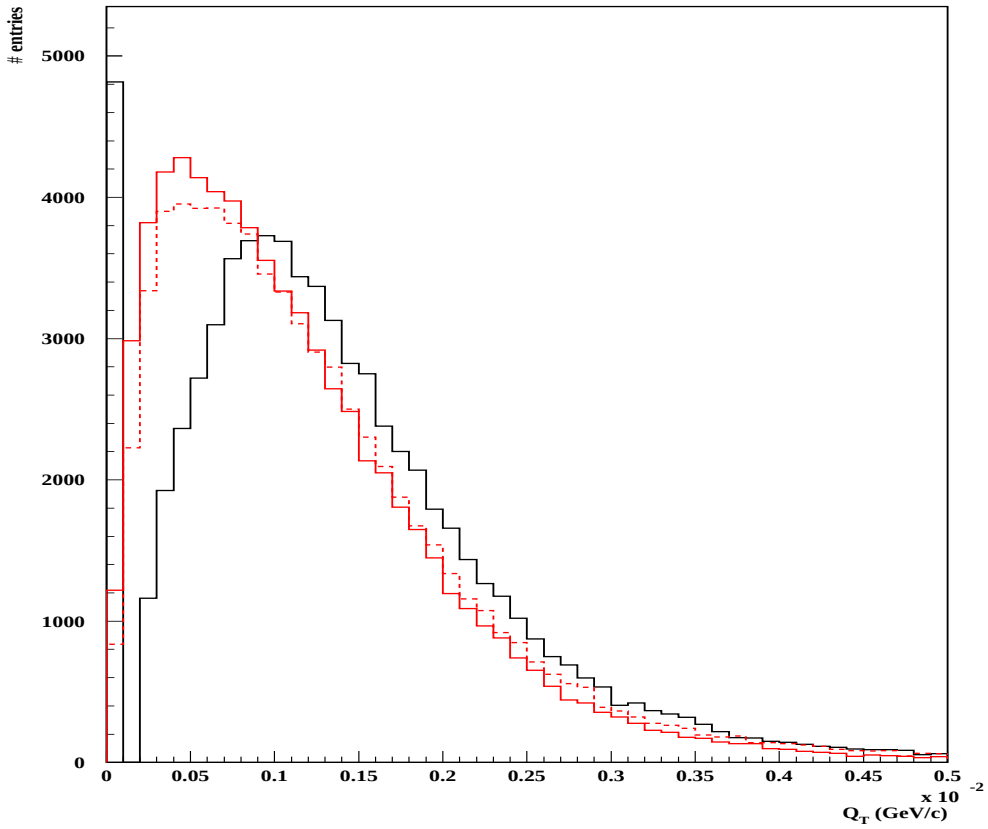

Fig. 14. *Reconstructed Q_T spectrum for atom pairs when only SFD hits are used in the final vertex fit (black). Full-tracking reconstruction is shown as dotted red line, and the true spectrum (G_1) is shown as a red line. The spike at zero corresponds to identical SFD hits.*

4.2 Coulomb pairs

Reconstruction of Coulomb pairs reveals sufficiently different properties so that they need be reported separately. Needless to say that the reconstruction package must be exactly the same in both cases. However, the Q_i span is much wider than for atom pairs, and that implies specific features that are presented in figures 1-10. We follow exactly the same exposure as previously done for atom pairs, and the results are presented at the bottom of each figure.

If we now review the general properties previously observed for atom pairs in $Q_{X,Y}$ reconstruction, we see that here too overall inefficiency does not exceed 5%. The resolution function defined by R_1/G_1 ratio has however a different shape. A narrow enhancement is observed at small $Q_{X,Y}$, which is actually the effect of SFD inefficiency. As a matter of fact, well separated track pairs will be reconstructed with a very small $Q_{X,Y}$ when one of the SFD hits is lost, and the MSGC is not able to recover the pair due to its own inefficiency [2]. The strong background of single-to-double ionisation in IH detector (at the level of 40%), and the fact that most pairs actually cross the same IH slab (standard reconstruction cut is $Q_T < 4$ MeV/c), makes the double ionisation cut rather inefficient to avoid this configuration. In $Q_T = \sqrt{Q_X^2 + Q_Y^2}$ spectrum this effect produces a smooth increase towards Q_T=0.

It is interesting to understand how the Q_X reconstruction performs for different number of MSGC+SFD hits in each track separately. There are 6 categories in total, namely 6-6, 6-5, 6-4, 5-5, 5-4 and 4-4. We show in figure 11 the reconstructed Q_X spectrum in each category, as compared with the original generator values, in each case. Like in the case of atom pairs, very short distances can be resolved by the MSGC in all categories, including 6-6. However, for the latter a bias exists against very small opening angles, due to the SFD double track resolution. The excess at zero Q_X corresponds to the fake pairs with one SFD hit missing, discussed in previous paragraph.

[2] note that $2\epsilon_s(1-\epsilon_s)+(1-\epsilon_s)^2 = 0.19$ for $\epsilon_s = 0.90$ being the single plane MSGC efficiency, and that two planes are required in this case.

5 Conclusions

The full-tracking method for DIRAC has been evaluated in detail with GEANT-DIRAC Monte Carlo data. Simulation of SFD, IH and MSGC detector backgrounds and efficiencies is complete, and background levels have been taken from previous works, using real data from 2001 runs, and they are rather accurate.

The results can be summarised as follows:

- The tracking is efficient for atoms and Coulomb pairs (maximum 5% overall inefficiency) and the original $Q_{X,Y}$ and Q_T spectra are well reconstructed in shape.
- resolution tails in all relevant transverse and longitudinal quantities have been determined, and they are all small (largest 3%).
- in particular, the loss of atom pairs after application of $Q_T > 4$ MeV/c cut is less than 2%.

Variation of detectors background and efficiencies within acceptable limits do not produce essential changes of the performance parameters analysed in this note.

The tracking method provides excellent resolution and performance for indistinct reconstruction of atom pairs and Coulomb pairs, and it is well suited for accurate determination of pionium lifetime.

References

[1] DIRAC note 03-08: A Tracking System for Upstream Detectors in DIRAC, B. Adeva, A. Romero and O. Vázquez Doce.

[2] B. Adeva et al. DIRAC : A High Resolution Spectrometer for Pionium Detection . NIM Nucl. Instr. Meth. A515 (2003) 467-496.

[3] M. Pentia, R. Muresan, A. G. Litvinenko, Nucl. Inst. and Meth. A 369 (1996) 101.

[4] M. Pentia and S. Constantinescu, "Uncertainties induced by multiple scattering in upstream detectors of the DIRAC setup", DIRAC Note 2001-04.

[5] DIRAC note 04-06 : Experimental determination of momentum resolution in DIRAC using Lambda events, B. Adeva, A. Romero and O. Vázquez Doce.

[6] B. Adeva et al., Detection of $\pi^+\pi^-$ atoms with the DIRAC spectrometer at CERN, J. Phys. G: Nucl. Part. Phys. 30 (2004) 1929.

[7] DIRAC note 02-01: The behaviour of the BASEL extended tracking and the standard ARIANE tracking to $A_{2\pi}$ Monte Carlo data in the DIRAC experiment, C. Shutz, L. Tauscher.

[8] DIRAC note 2002-09 : New Ionization Hodoscope: design and characteristics. V. Brekhovskikh, M. Jabitsky, A. Kuptsov, V. Lapshin, V. Rykalin, L. Tauscher.

[9] DIRAC note 04-02: DIRAC events generator, C. Santamarina.

[10] C. Santamaria, M. Schuman, L.G. Afanasyev, T. Heim, A Monte-Carlo Calculation of the Pionium Breakup Probability with Different Sets of Pionium Target Cross Sections, J. Phys. B. At. Mol. Opt. Phys. 36 4273 (2003), arXiv:physics/0306161 v1.

[11] DIRAC note 98-08. The GEANT-DIRAC Simulation Program Version 2.5. P. Zrelov and V. Yazkov.
http://zrelov.home.cern.ch/zrelov/dirac/montecarlo/instruction/instruct26.html

[12] http://dirac.web.cern.ch/DIRAC/pre-sel.html

[13] DIRAC note 05-11: Study of SFD Efficiency using MSGC Detector for 2001 Data , B. Adeva, A. Romero and O. Vázquez Doce.

[14] DIRAC note 04-03 : Dependence of breakup probability estimation on SCFi background, V.V. Yazkov.